C_{60} on alkali halides: Epitaxy and morphology studied by noncontact AFM

S. A. Burke, J. M. Mativetsky, S. Fostner, and P. Grütter
McGill University, Montreal, Quebec, Canada H3A 2T8

(Received 6 February 2007; revised manuscript received 30 April 2007; published 17 July 2007)

Submonolayer coverages of C_{60} deposited on KBr and NaCl are characterized by noncontact atomic force microscopy. Island shapes are described both qualitatively and quantitatively and their dependence on growth parameters and substrate is discussed. At room temperature, both compact and branched island morphologies are observed to coexist. An analysis of the island areas shows a distinct transition from compact to branched morphology with increasing island area. High-resolution imaging reveals differing coincident epitaxy at steps and on open terraces, despite consistent morphology for islands at both substrate positions. Molecular dewetting is proposed as a mechanism for the formation of branched islands.

DOI: 10.1103/PhysRevB.76.035419 PACS number(s): 68.37.Ps, 68.55.−a, 61.48.+c, 68.43.Hn

I. INTRODUCTION

Research into the optical and electronic properties of organic molecules, as well as the influence of structure on these properties, has received substantial interest in recent years due to the prospect of using molecules as active electronic and optoelectronic materials. The idea of fine-tuning the properties of single molecules and molecular materials through functionalization, as well as controlling self-assembly and tailoring structuring by customizing the intermolecular interactions and interactions with substrate structures,[1,2] gives molecules and molecular materials much of their promise as "building blocks" for electronic and optoelectronic devices. Though there has been a great deal of excitement regarding the promise of single molecule electronics, there remain formidable challenges in implementing reliable devices with the characteristics demanded by our current technological needs.[3] In parallel, thin-film organic electronics and optoelectronics have been developing, with some products already making their way into the marketplace,[4,5] though there remain challenges here as well in making organic devices competitive with current technologies.

In order to improve organic thin-film devices, growth and morphology of organic materials on inorganic surfaces have been studied extensively.[6,7] It has been shown that the structure of the films and the number and types of defects present are critically important to the properties to be exploited in device applications.[7,8] As such, understanding the growth of such films is crucial to the development of better devices.

However, even though insulators play an important role in most device structures, the majority of molecular studies have been conducted on metallic and semiconducting substrates. Difficulties with the use of typical electron-beam-based surface science tools on insulators include charging of the surface and electron-beam damages of the substrate.[2] Additionally, scanning tunnelling microscopy (STM), which has often been used for studies of molecules on surfaces,[9] requires some degree of conductivity of the substrate. In contrast, noncontact atomic force microscopy (nc-AFM) has demonstrated the ability to image insulating surfaces with atomic resolution[10] and has, in recent years, also been applied to a variety of molecular systems on insulating substrates with molecular resolution.[11–18] nc-AFM also allows characterization from the atomic and molecular scales up to the micron scale providing a connection between the molecular structure and the resulting morphology. This detailed structural characterization of such submonolayer molecular films is important to understanding the early stages of growth on insulators and the origins of defects in such films, as well as giving insight into the delicate balance between intermolecular interactions and substrate molecule interactions.

Submonolayer coverages of C_{60} on the (100) surfaces of alkali halides are examined herein. The alkali halides are ionic salts which can be readily cleaved along the (100) planes to produce atomically flat surfaces with large terraces suitable for growth studies. These surfaces have been studied in detail by nc-AFM,[10,19–21] such that preparation techniques and imaging conditions for atomic resolution are generally known. The C_{60} molecule has also been studied on a variety of surfaces, including several studies of film growth on alkali halides,[13,22–25] though the principle goal in many of these has been to achieve high-quality thick films. Submonolayer coverages, deposited at room temperature, of C_{60} on UHV-cleaved NaCl were observed by Lüthi *et al.*[25] with molecular resolution by AFM. Hexagonal and triangular islands typically two to three layers high were observed and found to nucleate predominately at step edges, and although atomic-scale resolution was obtained on both the C_{60} overlayer and NaCl substrate, no simple epitaxial relation could be determined. Kim *et al.*[22] used AFM to study the morphology of both islands and films of C_{60} on KBr grown at elevated substrate temperatures. At the lower coverages examined, they observed large crystalites with triangular and hexagonal edges and concave centers similar to those discussed here for high-temperature growth. Our own previous investigation[13] of submonolayer coverages of C_{60} deposited on room temperature, UHV cleaved KBr showed an unusual branched island morphology which had not been previously reported. The lack of explanation for these island shapes and their rather interesting form has compelled a more detailed investigation into the morphology and its connection, if any, to the atomic-scale structure of the crystallites, and is the topic of this paper. Here, both qualitative and quantitative characterizations of shape are used to examine the influence of growth parameters, namely, the deposition rate, coverage, substrate,

and temperature, on the resulting island morphologies. Energetic considerations and equilibrium morphology will also be addressed.

II. EXPERIMENTAL METHODS

The substrates used for this study are single-crystal alkali halides, specifically KBr and NaCl (Korth Kristalle, Germany). Both have a cubic rocksalt structure with (100) cleavage planes. The (100) planes exposed by cleaving consist of a square checkerboard pattern of positive (K+,Na+) and negative (Br−,Cl−) ions. Though similar in chemical composition, the lattice constant of the two surfaces differs by 1 Å with the conventional cell lattice constant of KBr being 6.6 Å and the lattice constant of NaCl being 5.6 Å with no significant deviation at the surface.[26,27] Substrate surfaces are prepared in ultrahigh vacuum (base pressure $<4\times10^{-8}$ Pa) by *in situ* cleaving using a cleaving stage (provided by JEOL) which presses a metal block against an extended piece of the bulk crystal allowing for a controlled break. Once cleaved, samples are heated to ~150 °C for 1 h. The substrate surface is then imaged with nc-AFM prior to deposition of molecules. KBr and NaCl (100) surfaces prepared in this way often exhibit atomically flat, defect-free terraces up to, and sometimes in excess of, 1 μm.

C_{60} obtained from Alfa Aesar (99.95%) is further purified by heating to 220 °C in vacuum for 14 h. Molecules are deposited *in situ* by thermal evaporation from quartz crucibles (Kentax, Germany) at 330 °C onto room temperature or heated substrates as prepared above. C_{60} molecules deposited on surfaces most often form a hexagonal structure corresponding to the (111) plane of the bulk fcc structure with lattice constants very similar to those in the bulk which exhibits a nearest-neighbor distance of 10.05 Å while the molecule itself has a van der Waals diameter of 7.1 Å.[28]

Samples were imaged at room temperature by a commercial JEOL JSPM 4500a AFM/STM in the noncontact mode. In nc-AFM imaging, the change in the resonance frequency caused by a tip-sample interaction of an oscillating cantilever is used to regulate distance as the tip is scanned over the surface. Topographic images are generated by maintaining a constant frequency shift.[29,30] A NanoSurf easyPLL was used for excitation and measurement of the frequency shift as well as feedback control to maintain constant oscillation amplitude. Nanosensors noncontact cantilevers (NCLR) were used which have a typical resonance frequency of 170 kHz and spring constant of 40–50 N/m. Typical oscillation amplitudes used were 6–7 nm.

III. RESULTS AND DISCUSSION

A. Morphology

On both KBr and NaCl, C_{60} exhibits an island growth mode for deposition onto a room-temperature substrate. Even at submonolayer coverages, molecular crystallites are two or more molecular layers high. Diffusion lengths on both substrates are estimated to be in the range of 600 nm–1 μm as reported previously for KBr.[13,23] The molecular islands predominantly nucleate at step edges on both surfaces, due in part to the large diffusion length and a preferred nucleation site at the step, particularly at kink sites.[13] The large diffusion length as well as an island growth mode indicate a relatively weak interaction with the surface on both substrates.

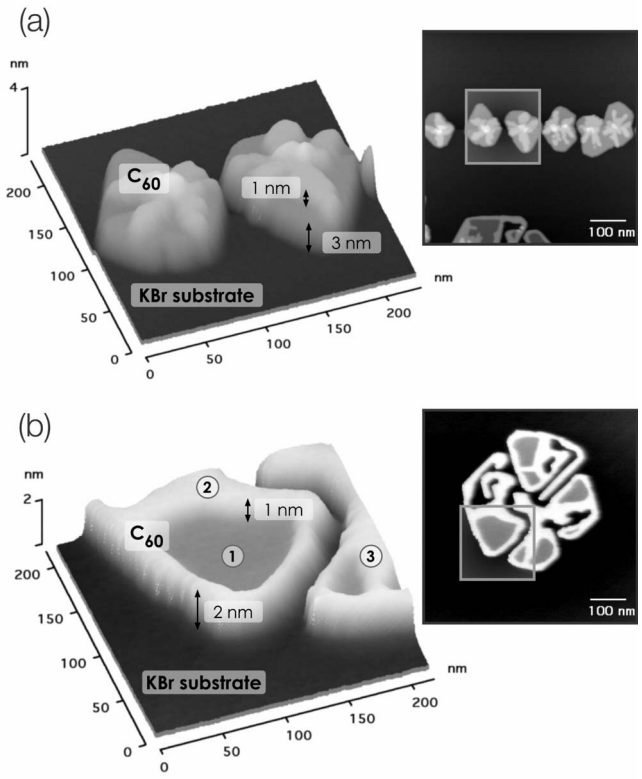

FIG. 1. Examples of the two island types observed: (a) compact multilayer islands with incomplete upper layers and (b) branched two-layer islands (2) with enclosed first layer regions (1) and disconnected regions (3).

In most cases, a combination of two different types of islands were observed after depositing C_{60} molecules: compact and branched (shown in Fig. 1). Compact islands maintain a generally hexagonal crystal border and are typically two or more layers tall, often with incomplete upper layers. Branched islands are generally two layers tall, often with enclosed first layer regions, and sometimes with incomplete additional layers. These islands maintain a hexagonal symmetry but also exhibit a dendriticlike branched structure. However, these branches often wrap back in toward the center of the island which is not characteristic of most dendritic structures. Additionally, these branched islands are often composed of disconnected regions which appear to be associated and have the same orientation with respect to the substrate. High-resolution imaging across a gap between disconnected regions confirms that the two separate pieces do indeed have the same orientational relation to the substrate (see Fig. 2).

On KBr, several different coverages and rates were examined (see Fig. 3 for an overview). There is little variation of the morphology with coverage. At lower coverages, the island sizes are smaller, approaching the branch width, and thus the branches are less extended making the islands appear more compact. For all coverages, a mixture of compact

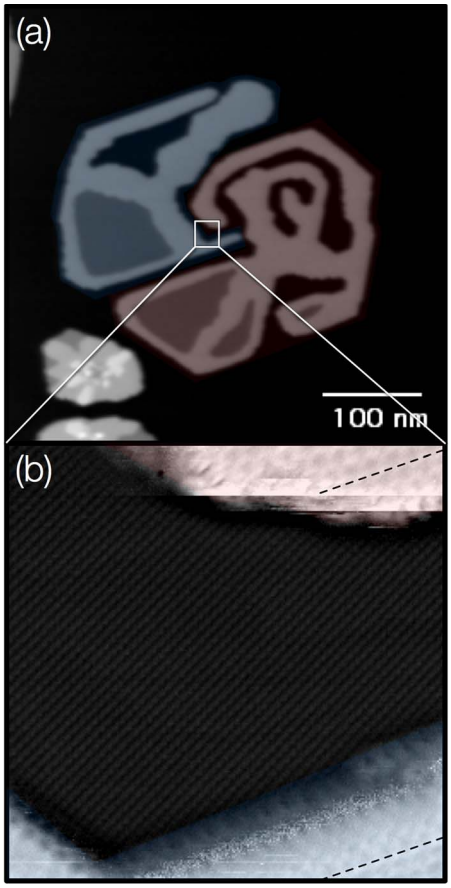

FIG. 2. (Color online) Island with two disconnected regions: (a) overview ($\Delta f=-1.9$ Hz, 440×440 nm^2) and (b) high resolution ($\Delta f=-13.0$ Hz, 20×20 nm^2, high pass filter+original image) showing alignment of molecular overlayer across the gap, dashed lines are parallel. Red and blue tinted regions in both images indicated the two disconnected regions, indicating that the top region of molecular contrast in (b) belongs to the lower right segment in (a) and the bottom region of molecular contrast is taken from an edge of the upper left segment in (a).

and branched islands could be observed. There is also little variation in the character of the growth over the accessible range of rates for the same coverage. Again, both branched and compact islands appear and there is no obvious difference in the degree of branching. It should be noted that the island size is influenced considerably by the substrate structure, mainly the density of steps. The images in Fig. 3 were selected to be representative of similar substrate areas. Some apparent differences in the island morphologies are a result of different local substrate morphology. For example, in the image shown for 0.1 ML at 0.0077 ML/s, the islands appear more compact. However, due to a higher density of steps in this region compared to some of the other areas shown for this coverage, the island sizes are smaller making them appear less branched. This effect, caused by the increased nucleation at step edges in combination with diffusion lengths often longer than terrace sizes, demonstrates the importance in preparing very clean flat surfaces for growth studies of these systems as well as understanding the role of steps and defects on film growth for device applications.

To quantify the shape information, the images were characterized based on perimeter and area measurements of individual islands. Figure 4 shows a typical dimensionality plot [log(area) vs log(perimeter)], or perimeter-area relation (PAR) plot, taken from measurements of many[31] islands from the same sample, i.e., identical rate and coverage. The most striking feature is a transition of the slope from a value of 2, as expected for compact shapes, to 0.9 ± 0.1. The value of this second slope is related to the fractal dimension by[32,33]

$$P=\alpha D' A^{D'/2}, \tag{1}$$

where P is perimeter, A is area, α is a constant, and D' is the fractal dimension of the two-dimensional island perimeter, yielding a fractal dimension of $D'=2.2\pm0.2$ corresponding to islands after the transition. Interestingly, the fractal dimension remains constant, within error, over all rates and coverages explored for both substrates indicating that the degree of branching is not significantly affected by the growth parameters, i.e., rate and coverage, or by the substrate.

The second parameter which can be extracted from the dimensionality plots is the island size at which the transition occurs (i.e., where the slope deviates from a value of 2). This transition area increases slightly with coverage for C_{60} on KBr [see Fig. 4(b)]. For islands on NaCl, the data show that the transition consistently occurs at larger area, i.e., islands are larger before becoming branched, and has a steeper dependence on coverage. No significant trend was distinguished for the dependence on rate. In contrast to the transition area, however, the branch width remains roughly constant regardless of coverage, rate, or substrate. Average values and standard deviations of measured branch widths were 27.1 ± 8.2 and 25.2 ± 8.7 nm for KBr and NaCl, respectively, with similarly small variations in the average value and the standard deviation for different rates and coverages.

The second characterization which has been applied is a dimensionless shape factor which is normalized to a circle (sometimes also referred to as the compactness):

$$\mathrm{SF}=\frac{4\pi A}{P^2}, \tag{2}$$

where A is the area and P is the perimeter. This gives a way to characterize how compact the shape is, and in the case of particular shapes, allows an identification of the shape, for example, a regular hexagon has $SF=0.906$. In the dimensionality plots, a change in compact shape would appear as a change in the intercept, with the same slope, whereas the shape factor would exhibit steps for changes in shape making such a transition easier to identify. A typical plot of the shape factor as a function of island area is shown in Fig. 5. For the C_{60} on KBr data analyzed, the shape factor indicates a roughly hexagonal shape for the compact region with no significant indication of a change in compact shape. After the transition to branched behavior, the curve follows the trend extracted from the dimensionality plots toward a linelike shape, or in terms of the branching, an increasing branch length with increasing the island size.

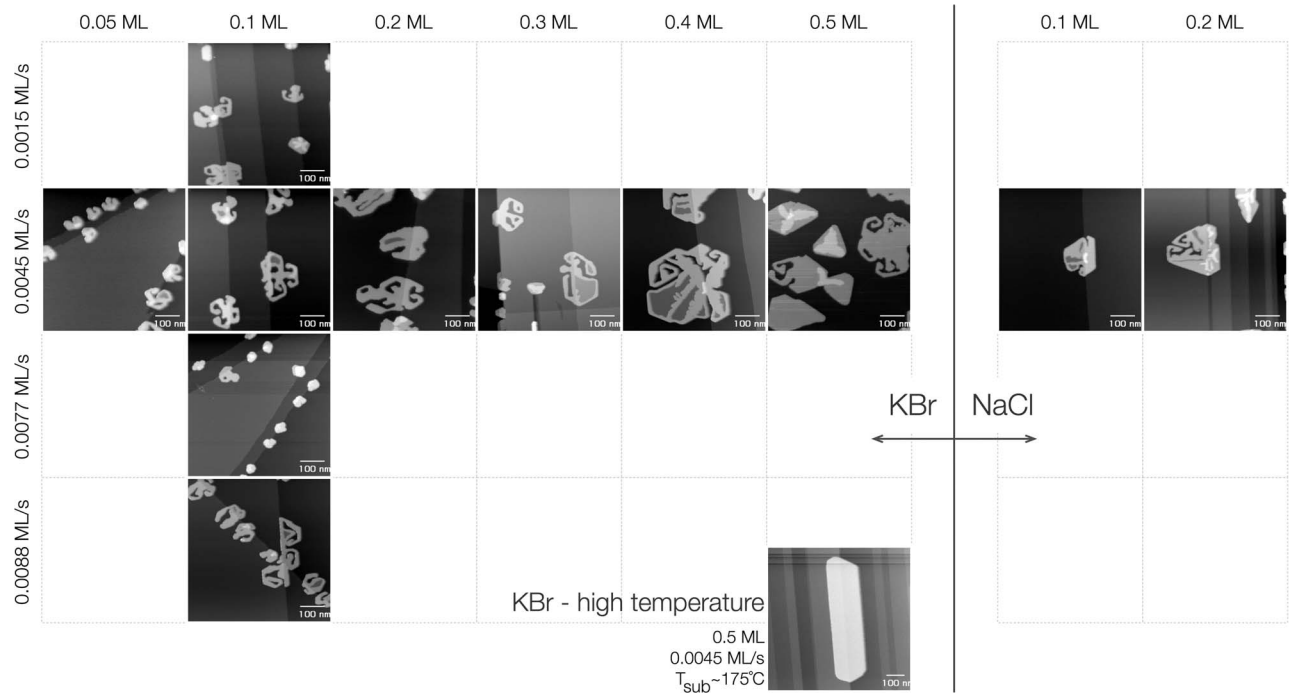

FIG. 3. Overviews with different rates, coverages, substrates, showing similar, representative areas. All images 600×600 nm^2.

Despite differences in orientation between islands nucleated at steps compared with those on free terraces, the trends in shape followed by the islands are the same regardless of where on the surface the island is located. The typical dimensionality plots shown in Figs. 4(a) and 5 include data points from both steps and terraces which clearly follow the same trend (see, in particular, the encircled points in Fig. 5). This indicates that the island shapes are not dependent on the details of nucleation or initial growth. This will be addressed further in relation to the molecular epitaxy.

B. Epitaxy on step and terrace on KBr

The high-resolution imaging capability of the nc-AFM technique allows for real-space determination of surface structures. In particular, if both the overlayer and substrate structure can be resolved, the lattice parameters of the overlayer can be corrected for any drift, creep, or nonlinearities in the piezo, thus improving the confidence in the measured lattice constants. In many cases, determination of the overlayer relation to the substrate is only possible when the substrate is also resolved, as the uncertainty in the measured lattice constants may be too large to ascribe a unique superstructure, especially for large epitaxial cells.

nc-AFM topographic images showing resolution on both the substrate and the overlayer [see Fig. 6(a)] over the edge of an island situated on a terrace are used to determine the overlayer relation to the substrate. As the KBr lattice parameters are well known,[27] the lattice parameters measured from the image are used as a calibration and the determined transformation is then used to correct all other measurements within the image. Measuring the C_{60} lattice and applying the appropriate correction yield lattice constants of $b_1=10.3\pm0.2$ Å and $b_2=9.8\pm0.4$ Å with an angle between the two lattice vectors of $\beta=61\pm2°$. The rotation of the overlayer lattice relative to the $\langle100\rangle$ direction of the conventional unit cell of the KBr is also measured and corrected and found to be $\theta=17.1\pm0.7°$. Using these lattice constants and the overlayer rotation, with the known lattice constants of KBr, one can calculate the expected transformation matrix which describes the overlayer relation defined as[34]

$$\begin{bmatrix}\mathbf{b}_1\\ \mathbf{b}_2\end{bmatrix}=[\mathbf{C}]\begin{bmatrix}\mathbf{a}_1\\ \mathbf{a}_2\end{bmatrix}=\begin{bmatrix}p & q\\ r & s\end{bmatrix}\begin{bmatrix}\mathbf{a}_1\\ \mathbf{a}_2\end{bmatrix}, \tag{3}$$

where the $\mathbf{b}_i$ are the molecular overlayer lattice vectors, and the $\mathbf{a}_i$ are the substrate lattice vectors. Classification of the type of epitaxy can be made from the matrix elements p,q,r,s, which define the positions of the adsorbates relative to the substrate. In molecular epitaxy, coincident structures are far more common than in inorganic epitaxy and there are several subclassifications which can be made (see Refs. 34 and 35).

In this case, the matrix calculated from the measured and corrected lattice parameters gives the coincident relation,

$$\mathbf{C}=\begin{pmatrix}1.49\pm0.03 & 0.46\pm0.02\\ 0.31\pm0.06 & 1.45\pm0.06\end{pmatrix}. \tag{4}$$

In high-resolution images of first layer C_{60} regions, a long-range periodicity is observed with a weak corrugation of ~10 pm compared to the C_{60} corrugation of around 20 pm. If it is assumed that this moiré pattern is a result of the overlayer-substrate correspondence, then it can also be used to arrive at the transformation matrix. The periodicity of the observed moiré can be described by a new set of lattice vectors in terms of the C_{60} lattice vectors,

$$\mathbf{c}_1=10\mathbf{b}_1, \tag{5}$$

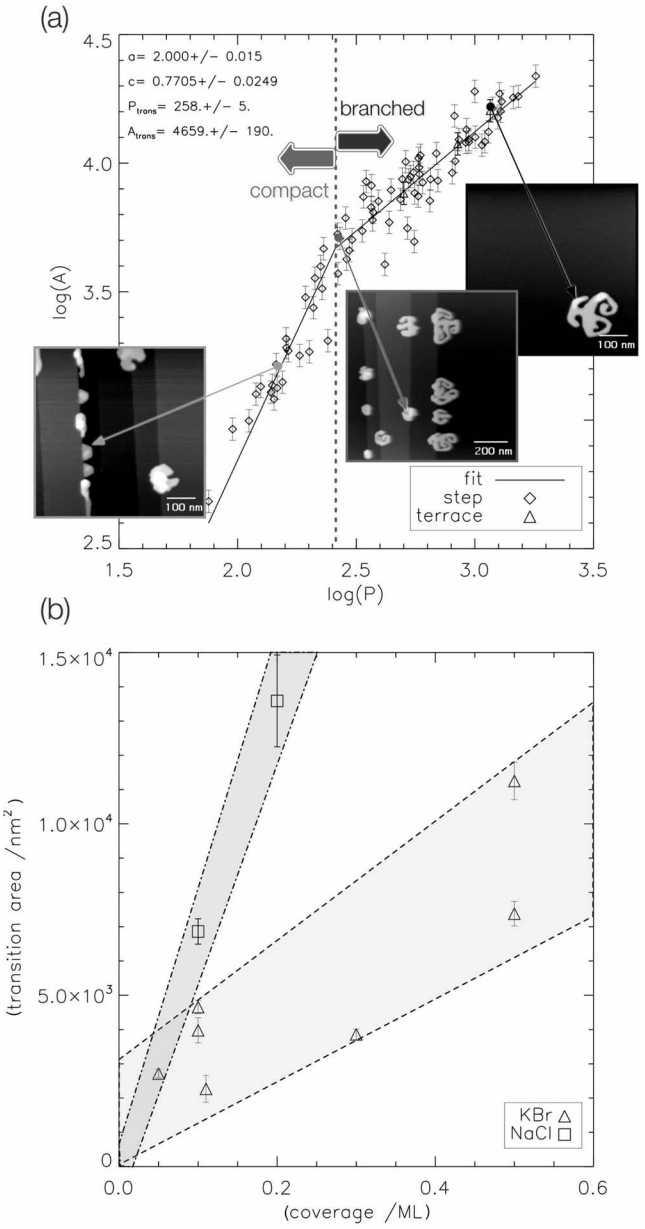

FIG. 4. The plot in (a) shows a typical dimensionality plot for a particular rate and coverage (~0.004 ML/s, 0.1 ML). Images of the particular islands corresponding to points on the graph are shown for three key regions: the compact, slope=2 region, near the transition, and above the transition where branching is fully developed. The parameters in the upper left corner are defined as follows: a and c are the slopes for the compact and branched regions, respectively, and P_{trans} and A_{trans} are the perimeter and area, respectively, at which the transition occurs. The plot in (b) summarizes the area at which the transition occurs as a function of coverage and shows the difference in trends for KBr and NaCl, represented approximately by the gray areas.

$$\mathbf{c}_2 = -3\mathbf{b}_1 + 7\mathbf{b}_2. \tag{6}$$

Using the calibrated C_{60} lattice constants and measured angle of the overlayer with respect to the KBr to determine the moiré pattern in terms of the KBr lattice and equating the two, one arrives at the transformation matrix giving

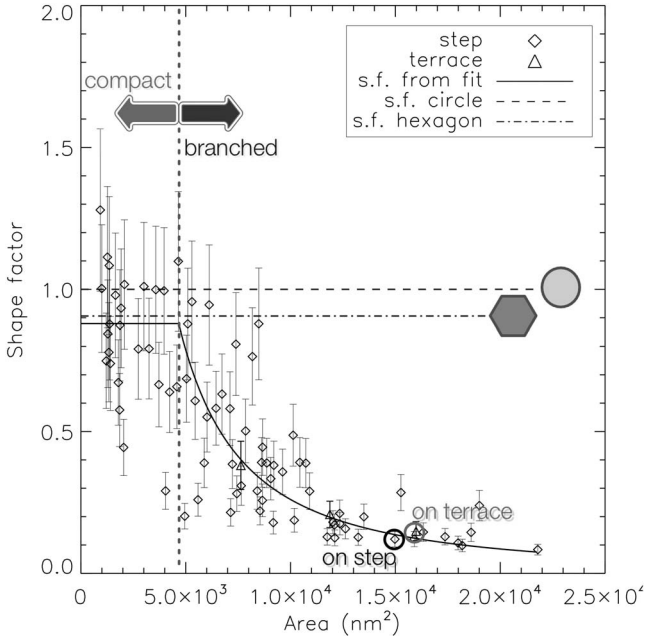

FIG. 5. Typical plot of the shape factor [see Eq. (2)] as a function of island area for the same sample shown in Fig. 4(a). Up to the transition area, denoted by the vertical dashed line, the shape is roughly hexagonal. At areas greater than the transition area, the shape approaches SF=0, or "linelike." The solid line corresponds to the fit from the dimensionality plot in Fig. 4(a). The two encircled points show islands with both similar areas and similar shapes one of which was positioned at a step and the other positioned on an open terrace.

$$\mathbf{C} = \begin{pmatrix} 1.48 \pm 0.03 & 0.45 \pm 0.01 \\ 0.30 \pm 0.01 & 1.44 \pm 0.06 \end{pmatrix}. \tag{7}$$

As the two matrices agree to within the small errors on each of the matrix elements, it is likely that the observed long-range periodicity is caused by overlayer-substrate correspondence. Possible mechanisms for the observed moiré contrast in the nc-AFM topography include geometrical effects, where the C_{60} lattice is in and out of registry with the KBr lattice minima and electrostatic effects caused by the interaction of the molecules with the underlying ionic lattice. From the matrix elements found, there are two possible coincident structures that are consistent with the periodicity of the moiré within the range of errors given for the matrix elements,

$$\begin{pmatrix} 3/2 & 9/20 \\ 2/7 & 207/140 \end{pmatrix}, \begin{pmatrix} 3/2 & 9/20 \\ 2/7 & 197/140 \end{pmatrix}. \tag{8}$$

The first of these is shown in Fig. 6(c). As it corresponds to C_{60} lattice constants which are more similar to the equilibrium spacing of C_{60}, it is a more likely structure given the weak interaction between C_{60} and KBr, though the two cannot be distinguished by the measurements presented here. In both cases, the periodicity of the moiré [shown in Fig. 6(c) by the gray dashed line] does not correspond to an integer number of KBr lattice constants, but rather 1/2-integer values corresponding to the position of the opposite ion. This

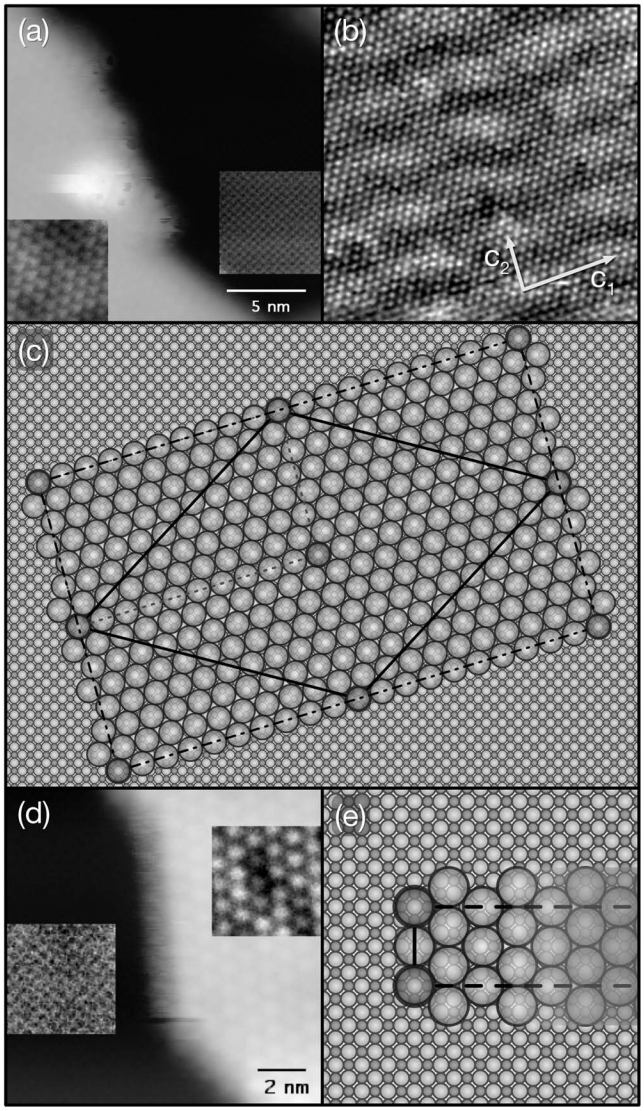

FIG. 6. High-resolution imaging of an island found on an open terrace are shown over the edge of the island with KBr resolution in (a) ($\Delta f=-13.0$ Hz, 20×20 nm^2), and on a first layer region in (b) ($\Delta f=-7.0$ Hz, 30×30 nm^2) with the vectors c_1 and c_2 representing the periodicity of the moiré. The corrugation of the moiré is ~10 pm, with a C_{60} corrugation of ~20 pm. One of two possible coincident structures is shown in (c) based on high-resolution imaging. High-resolution imaging over the edge of an island found adjacent to a step is also shown in (d) ($\Delta f=-11.3$ Hz, 13×13 nm^2) (Ref. 13) with the corresponding $n\times3$ structure observed in (e).

tends to support a geometrical rather than an electrostatic mechanism for the observed contrast, as the contrast would be expected to differ over opposite ions if it were a purely electrostatic effect. It is hoped that detailed modeling of the overlayer structure and simulation of nc-AFM imaging of such an overlayer structure will shed light on the mechanism responsible for the observed moiré pattern.

The relation of the C_{60} overlayer to the KBr substrate for an island located at a step was previously reported.[13] In this case, a coincident epitaxy was determined with an 8×3 supercell. As the long direction of the supercell could not be determined exactly from the measured lattice constants, an energetic consideration of possible cells was used to determine the most likely structure. In similar situations where islands are found at ⟨100⟩ steps, other $n\times3$ structures have been observed, where in the direction of the step there is an alignment with the KBr and two molecules for every three KBr conventional unit cells [shown schematically in Fig. 6(e)]. In the direction which is not aligned, there seems to be some freedom for different structures to occur. This alignment with the ⟨100⟩ direction is in contrast to islands found on free terraces which show some rotation relative to the KBr lattice. This clearly indicates that the nearby ⟨100⟩ step influences the epitaxy by forcing an alignment of one of the overlayer lattice vectors with this direction.

It is interesting to note that although the epitaxy for molecular islands on open terraces and at steps differs significantly, the large scale morphology, as stated previously, follows the same trend irrespective of location on the substrate. Additionally, the behavior on NaCl, which has a smaller lattice constant compared to KBr, is also strikingly similar. Although simultaneous resolution on C_{60} and NaCl was not obtained, the epitaxy will by necessity also be somewhat different to fit the underlying substrate lattice. The lack of a connection between the morphology and the atomic/molecular scale features indicates that the mechanism responsible for the island shapes is dictated by a larger scale, collective interaction.

C. Energetics and dynamics of growth

To explore the energy landscape of the growth, C_{60} was deposited on KBr, using the same coverage and rate, either onto a heated substrate or onto a room-temperature substrate and later annealed or allowed to age. A coverage of 0.5 ML of C_{60} was deposited at a rate of 0.0045 ML/s on a KBr substrate held at 175 °C, shown in Fig. 7(b) as well as in the lower inset of Fig. 3. Compact islands ranging in shape from elongated hexagonal crystals to nearly triangular crystals with heights greater than 4 nm were observed. Distances between islands were often larger than 1 μm despite intervening steps due to the increased diffusion on the surface at elevated temperature. These observations, particularly the island shapes, are consistent with previously reported results for C_{60} on KBr at elevated temperature.[22] As compared to the growth at room temperature for the same coverage and rate which exhibits the branched island morphology described in Sec. III A, and shown in Fig. 7(a), the island morphology is significantly influenced by the substrate heating.

In contrast, though annealing does have some effect, the islands do not transform to a compact island morphology. The room-temperature deposited sample shown in Fig. 7(a) was heated to 175 °C for 16 h. The sample after annealing, shown in Fig. 7(c), does not contain any first layer enclosed areas as observed prior to annealing, indicating that this first layer region is metastable. A similar effect can be noted in an aged sample (nine days after deposition), shown in Fig. 7(d), where the majority of interior holes do not contain any first layer C_{60} and the small portions that are observed are broken up and surrounded by small branches.

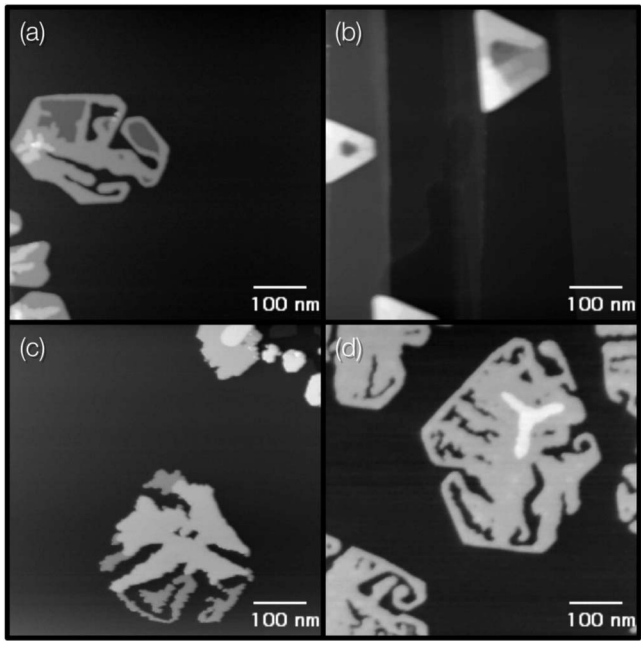

FIG. 7. (a) 0.5 ML C_{60} deposited at 0.0045 ML/s on KBr at room temperature (Z_{max}=4.79 nm), (b) 0.5 ML C_{60} deposited at 0.0045 ML/s on KBr at 175 °C (Z_{max}=16.6 nm), (c) same sample as shown in (a) after annealing at 175 °C for 16 h (Z_{max} =5.63 nm), and (d) 0.5 ML C_{60} deposited at 0.0045 ML/s without annealing, aged for nine days (Z_{max}=3.39 nm). Though annealing, and similarly aging, has some effect on the structure, the overall branched morphology remains, whereas depositing molecules onto a heated substrate results in a compact island morphology.

Additionally, after annealing, there is evidence of some evaporation from the edges of the island exhibited by the increased roughness of the island edges. Annealing of a different sample to 250 °C for 16 h resulted in complete evaporation of the C_{60} from the surface. Although there may be an intermediate temperature where annealing causes a change in morphology from branched to compact islands, the evidence of some degree of initial evaporation even at the lower annealing temperature indicates that the barrier to the rearrangement of existing branched islands is quite large, and possibly even similar to the desorption energy. In other words, the branched structures are relatively stable once formed, due to a significant C_{60}-C_{60} interaction in comparison with the binding to the substrate and an inability even at this elevated temperature to achieve sufficient long-range diffusion to enable such a rearrangement. However, when the system is given more energy during growth, as in the case of a heated substrate, the islands form compact shapes and this is taken to be the equilibrium morphology.

The detailed mechanism for creating the branched structures observed has yet to be determined. Generally, fractal or branched structures caused by a "hit and stick" or limited edge and/or corner diffusion do not exhibit branches which wrap back toward the center of the island.[36] Rather, those structures tend to branch outward from a central nucleation point, unlike those seen here. The different appearance and correspondingly different fractal dimension make this kind of growth mechanism an unlikely candidate for the formation of the structures formed by the C_{60} deposit.

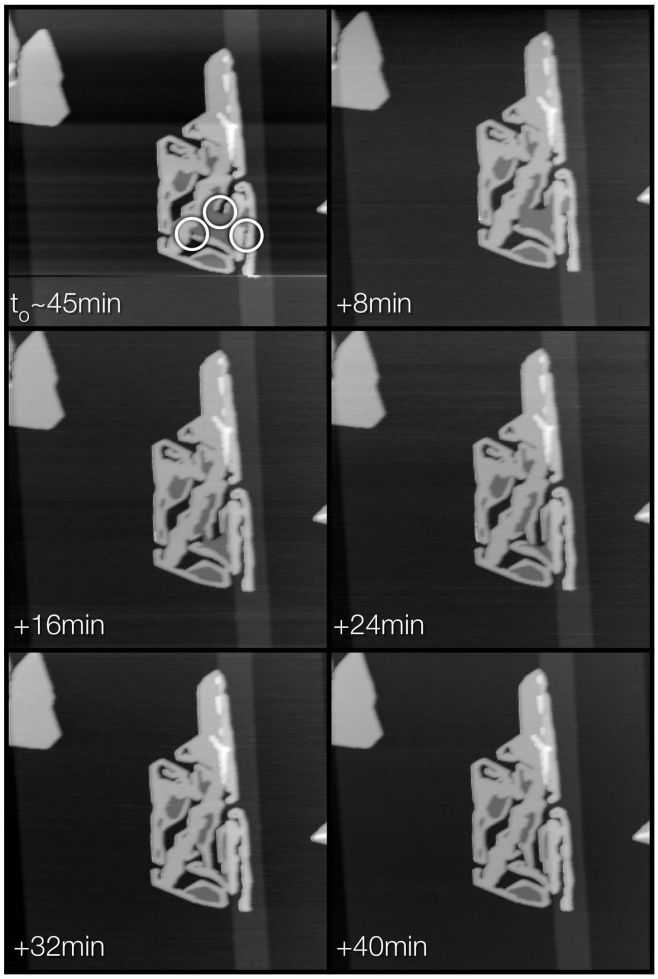

FIG. 8. Sequence of nc-AFM images shortly after deposition showing dynamics of the island morphology. The first images was acquired ~45 min after deposition. Three areas where a first layer edge is exposed are encircled. Subsequent images were taken ~8 min apart and the time from the first image is indicated. The exposed first layer region receeds from the edge building up a second layer rim. Once enclosed, the remaining first layer regions are stable, as are the two layer branches. $\Delta f \simeq -2.8$ Hz, 600 $\times$ 600 nm^2.

An indication of a suitable mechanism comes from a series of images acquired before the structures had completed formation, seen in Fig. 8. The first of these images was taken ~45 min after deposition of C_{60} onto NaCl, and shows three areas of first layer C_{60} which are *not* enclosed by a second layer rim, as was shown and discussed for typical stable islands at later time [e.g., Fig. 1(b)]. As indicated by the annealing and late-time observations, that the first layer is unstable, these exposed first layer areas are seen to recede from the edge in the subsequent images. At the same time as the first layer recedes, a second layer rim is built up which protects portions of the remaining first layer. The result, ~40 min after the first image of the sequence was taken, is a stable structure exhibiting branching, enclosed first layer regions, and two very nearly disconnected portions of the is-

land, all of the features which have been observed for this type of island. Note that tip-induced forces can be excluded as the cause of the changes observed on the basis that such dynamics were not observed during normal imaging of later time stable islands.

This dynamical sequence indicates that the branched island growth may occur by an initial wetting of the alkali halide surface by single layer islands of C_{60} followed by a dewetting, which due to additional factors, such as instabilities in the receding film edge and limited long-range diffusion, forms the observed stable branched structures. The proposed process would proceed from the formation of large single layer islands during deposition. After the deposition is completed, this single molecular layer would destabilize at the edges. These edge molecules, which have a lower coordination, could diffuse along island edges, across corners, on top of the existing layer, or away from the island. Though each of these processes occurs on very short time scales, each has a different probability associated with it, and each of many molecules must undergo such processes until a stable configuration is reached.[37,38] The net result is a collective rearrangement process which would take significantly longer than the individual molecular motions allowing for observation of the structural changes. Those molecules which diffuse on top of the existing single layer can form a second layer rim which increases the coordination of the edge and appears to stabilize both the edge and the enclosed single layer region. The images shown here are assumed to be at a late stage of this rearrangement when most of the island structure is established, but some unstable regions remain and these are observed to change. It should be noted that although stable for a much longer time, the enclosed first layer also breaks and proceeds to dewet as seen for aged islands [Fig. 7(d)], despite the greater coordination of the molecules within a layer compared to the first layer edge.

The formation of disconnected regions of island groups, and the seeming "communication" between these regions which exhibit the same orientation with respect to the substrate (see Fig. 2), is readily explained by such a dewetting process. These related regions are initially part of the same single layer island whereby the orientation is set and later becomes disconnected through the dewetting of the film. Additionally, the epitaxy of the film is not expected to play a significant role as the interaction with the substrate in such a situation where dewetting occurs must be weak. Thus, the observation that the epitaxy has little to no influence on the morphology, as shown by the uniform morphology at steps and terraces despite differing epitaxy, is also consistent with a dewetting scenario.

Although dewetting does not directly account for the formation of the branched island structures observed, similar morphologies have been observed previously as a result of dewetting phenomena. Dewetting has recently been reported in several systems of organic molecules deposited by organic molecular beam deposition on inorganic substrates,[39–42] and, in particular, the "skeleton" island morphology described by Witte *et al.* for perylene on Cu(110) (Ref. 44) exhibits some similar features to those described here. The thick branches and holes, though somewhat different than those described here due to a square rather than hexagonal symmetry, are visually similar. Also, the fairly uniform height of the observed branched islands and characteristic rim structures, which they suggest may be a result of a diffusion barrier at the edge of the island, are both features observed here for C_{60}. The presence of these similarities in conjunction with the direct observation of a single layer film receding to form these features strongly points to the occurrence of dewetting.

Furthermore, the details of the individual molecular processes mentioned above with the relative time scales and probabilities of each are likely responsible for the details of the final morphology. As such, the subtle differences in morphology between the two different substrates investigated are likely a result of differences in the molecular scale diffusion processes on each surface. Instabilities in the dewetting process, occurring on the length scale given by the transition from compact to branched islands, may initiate the formation of the branches. Though relatively fast short-range diffusion can easily accomplish local stability, producing crystallographic edges and the two layers which seem to be required for stability, it appears that there is insufficient mobility to fill in voids and troughs between branches at room temperature within reasonable experimental time scales to allow the system to reach the global equilibrium state of compact islands.[37,38]

In most cases, dewetting of a film is initiated by an increase in temperature or some other change in conditions after or during the initial deposition of the film. However, as growth is a nonequilibrium process, due to the flux of particles impinging on the sample, it is possible that a single layer film could become favorable during growth, whereas island growth may be favorable in the equilibrium case. For example, the balance of surface energies may differ during and after growth due to the flux of particles incident on the sample (which can also be interpreted as a background vapor pressure).[43,44] Should this occur, a layer growth mode may be favorable despite an anticipated island growth mode. However, upon ceasing exposure to the source, the balance of surface energies would shift back to favor an island growth mode, and one might expect the film to spontaneously dewet causing the structures to change shortly after deposition.

IV. SUMMARY AND CONCLUSIONS

nc-AFM has been used here as a surface science tool capable of bridging the characterization gap from the molecular scale up to the micron scale allowing connections between epitaxy and crystal structure to growth and morphology. Combined with quantitative characterizations of shape, this allows study of collective mechanisms, such as dewetting, and consideration of the effects of atomic and molecular scale interactions on such processes.

Molecular islands of C_{60} deposited on both the alkali halides KBr and NaCl exhibit a branched morphology above a critical transition area. These unusual morphologies are most likely a result of dewetting phenomena, though other factors related to diffusion and instabilities in the process presumably play a role in the resulting final shapes observed. Due to the domination of intermolecular interactions over molecule-

substrate interactions and the collective nature of dewetting, the morphologies are seemingly unaffected by the differing epitaxies observed for islands on open terraces and those guided by ⟨100⟩ steps. The similar morphology observed on the two different substrates also exhibits only subtle differences, as seen in the dependence of the transition area on coverage, whereas many aspects, such as the branch widths and fractal dimension observed, are strikingly similar again pointing to the limited role played by the substrate in the formation of the island shapes. The occurrence of dewetting in this system also gives an explanation for how disconnected regions of the same island group are observed to have the same orientation with respect to the substrate, as the regions would have been connected by a single layer at an earlier stage of the growth. In recent years, dewetting has become increasingly identified as an important process in the growth of many organic films on metals, and may also be a significant consideration in the growth of molecular deposits on insulators.

ACKNOWLEDGMENTS

The authors would like to thank Jorge Viñals for fruitful conversations regarding growth morphologies, and gratefully acknowledge the following funding agencies for their support: NSERC, CIAR, FQRNT, and CFI.

[1] J. Barth, G. Costantini, and K. Kern, Nature (London) **437**, 671 (2005).
[2] R. Bennewitz, J. Phys.: Condens. Matter **18**, R417 (2006).
[3] S. Lindsay and M. Ratner, Adv. Mater. (Weinheim, Ger.) **19**, 23 (2007).
[4] C. Dimitrakopoulos and P. Malenfant, Adv. Mater. (Weinheim, Ger.) **14**, 99 (2002).
[5] J. Sheats, J. Mater. Res. **19**, 1974 (2004).
[6] S. Forrest, Chem. Rev. (Washington, D.C.) **97**, 1793 (1997).
[7] G. Witte and C. Wöll, J. Mater. Res. **19**, 1889 (2004).
[8] N. Karl, Synth. Met. **133-134**, 649 (2003).
[9] F. Rosei, M. Schunack, Y. Naitoh, P. Jiang, A. Gourdon, E. Laegsgaard, I. Stensgaard, C. Joachim, and F. Besenbacher, Prog. Surf. Sci. **71**, 95 (2003).
[10] M. Bammerlin, R. Lüthi, E. Meyer, A. Baratoff, J. Lü, M. Guggisberg, C. Loppacher, C. Gerber, and H.-J. Güntherodt, Appl. Phys. A: Mater. Sci. Process. **66**, S293 (1998).
[11] T. Fukuma, K. Kobayashi, K. Noda, K. Ishida, T. Hoiruchi, H. Yamada, and K. Matsushige, Surf. Sci. **516**, 103 (2002).
[12] L. Nony, E. Gnecco, A. Baratoff, A. Alkauskas, R. Bennewitz, O. Pfeiffer, S. Maier, A. Wetzel, E. Meyer, and C. Gerber, Nano Lett. **4**, 2185 (2004).
[13] S. A. Burke, J. M. Mativetsky, R. Hoffmann, and P. Grütter, Phys. Rev. Lett. **94**, 096102 (2005).
[14] T. Kunstmann, A. Schlarb, M. Fendrich, T. Wagner, R. Möller, and R. Hoffmann, Phys. Rev. B **71**, 121403(R) (2005).
[15] O. Pfeiffer, E. Gnecco, L. Zimmerli, S. Maier, E. Meyer, L. Nony, R. Bennewitz, F. Deiderich, H. Fang, and D. Bonifazi, J. Phys.: Conf. Ser. **19**, 166 (2005).
[16] C. Loppacher, U. Zerweck, L. Eng, S. Gemming, G. Seifert, C. Olbrich, K. Morawetz, and M. Schreiber, Nanotechnology **17**, 1568 (2006).
[17] U. Zerweck, C. Loppacher, and L. Eng, Nanotechnology **17**, S107 (2006).
[18] J. Mativetsky, S. Burke, S. Fostner, and P. Grütter, Nanotechnology **18**, 105303 (2007).
[19] R. Bennewitz, O. Pfeiffer, S. Schär, V. Barwich, E. Meyer, and L. Kantorovich, Appl. Surf. Sci. **188**, 234 (2002).
[20] R. Hoffmann, L. N. Kantorovich, A. Baratoff, H. J. Hug, and H.-J. Güntherodt, Phys. Rev. Lett. **92**, 146103 (2004).
[21] M. A. Lantz, R. Hoffmann, A. S. Foster, A. Baratoff, H. J. Hug, H. R. Hidber, and H.-J. Güntherodt, Phys. Rev. B **74**, 245426 (2006).
[22] Y. Kim, L. Jiang, T. Iyoda, K. Hashimoto, and A. Fujishima, Appl. Surf. Sci. **130-132**, 602 (1998).
[23] K. Yase, N. Ara-Kato, T. Hanada, H. Takiguchi, Y. Yoshida, G. Back, K. Abe, and N. Tanigaki, Thin Solid Films **331**, 131 (1998).
[24] K. Tanigaki, S. Kuroshima, and T. Ebbesen, Thin Solid Films **257**, 154 (1995).
[25] R. Lüthi, H. Haefke, E. Meyer, L. Howald, H.-P. Lang, G. Gerth, and H.-J. Güntherodt, Z. Phys. B: Condens. Matter **95**, 1 (1994).
[26] J. Vogt and H. Weiss, Surf. Sci. **491**, 155 (2001).
[27] J. Vogt and H. Weiss, Surf. Sci. **501**, 203 (2002).
[28] L. A. Girifalco, J. Phys. Chem. **96**, 858 (1992).
[29] S. Morita, R. Weisendanger, and E. Meyer, *Non-Contact Atomic Force Microscopy* (Springer, Berlin, 2002).
[30] T. Albrecht, P. Grütter, D. Horne, and D. Rugar, J. Appl. Phys. **68**, 668 (1991).
[31] A total of 611 islands were parametrized using the JEOL WINSPM software. These islands were taken from nine different samples, 17–90 islands from each sample, representing different preparation conditions. To avoid systematic error introduced by inaccuracies in the area and perimeter measurement algorithms, islands with areas in pixels less than 100 were excluded. By using the area in pixels as the cutoff, differences between image sizes are also reduced (above the cutoff, the differences for the same island are within the given error bars).
[32] J. M. Gómez-Rodríguez, A. M. Baró, L. Vázquez, R. C. Salvarezza, J. M. Vara, and A. J. Arvia, J. Phys. Chem. **96**, 347 (1992).
[33] J. Williams and T. Beebe, Jr., J. Phys. Chem. **97**, 6255 (1993).
[34] D. E. Hooks, T. Fritz, and M. D. Ward, Adv. Mater. (Weinheim, Ger.) **13**, 227 (2001).
[35] S. C. B. Mannsfeld, K. Leo, and T. Fritz, Phys. Rev. Lett. **94**, 056104 (2005).
[36] Z. Zhang and M. Lagally, Science **276**, 377 (1997).
[37] K. Binder, Phys. Rev. B **15**, 4425 (1977).
[38] W. Mullins and J. Viñals, Acta Metall. **37**, 991 (1989).
[39] B. Krause, A. Dürr, F. Schreiber, and H. Dosch, J. Chem. Phys. **119**, 3429 (2003).
[40] Y. Tang, Y. Wang, G. Wang, H. Wang, L. Wang, and D. Yan, J. Phys. Chem. B **108**, 12921 (2004).
[41] G. Witte, K. Hänel, S. Söhnchen, and C. Wöll, Appl. Phys. A: Mater. Sci. Process. **82**, 477 (2006).
[42] S. Rath and H. Port, Chem. Phys. Lett. **421**, 152 (2006).
[43] P. Tarazona and R. Evans, Mol. Phys. **48**, 799 (1983).
[44] P. deGennes, Rev. Mod. Phys. **57**, 827 (1985).